

# Feasibility Study on the Use of Near-Infrared Hyperspectral Imaging for the Screening of Anthocyanins in Intact Grapes during Ripening

José Miguel Hernández-Hierro, Julio Nogales-Bueno, Francisco José Rodríguez-Pulido, and Francisco José Heredia\*

Food Colour and Quality Laboratory, Department of Nutrition and Food Science, Facultad de Farmacia, Universidad de Sevilla, 41012 Sevilla, Spain.

**ABSTRACT:** The potential of near-infrared hyperspectral imaging to determine anthocyanins in intact grape has been evaluated. The hyperspectral images of intact grapes during ripening were recorded using a near-infrared hyperspectral imaging covering the spectral range between 900 and 1700 nm. Reference values of anthocyanins were obtained by HPLC-DAD. A number of spectral pretreatments and different mask development strategies were studied. Calibrations were performed by modified partial least-squares regression (MPLS) and present a good potential (RSQ of 0.86 and SEP values of 2.62 and 3.05 mg g<sup>-1</sup> of grape skin for nonacylated and total anthocyanins, respectively) for a fast and reasonably inexpensive screening of these compounds in intact grapes.

**KEYWORDS:** phenolic compounds, anthocyanins, grapes, hyperspectral imaging, near-infrared, chemometrics

## ■ INTRODUCTION

Phenolics are secondary metabolites that play important roles in the plant kingdom.<sup>1,2</sup> Among them, anthocyanidins are responsible for tissue pigmentation and provide colors that range from reddish to purplish ones.<sup>1</sup> Grapes are a nonclimateric fruit that follow three growing phases and contain several phenolic compounds, which include anthocyanins in the case of red cultivars. Anthocyanins are responsible for the color of red wines, and their interactions with other phenolic compounds largely determine the color changes observed during aging.<sup>3–5</sup> Furthermore, the influence of anthocyanins in the antioxidant activity of red wines has also been previously reported.<sup>6</sup> Biosynthesis and accumulation of anthocyanins in red grape skins start at veraison (the interception between phases II and III),<sup>7</sup> and factors such as cultivar, growing region, climate, and growth conditions may influence the levels of anthocyanins.<sup>8–14</sup> In warm climate regions, the aforementioned compounds are negatively influenced by high solar radiation exposures and temperatures, which are high not only during the day but also during the night.<sup>15</sup> In that case, grape cultivar selection is extremely important in facing future problems with color quality and stability of red wines obtained from these berries.<sup>8</sup> Moreover, deciding on the optimal harvest time with regard to anthocyanins is a great concern for wineries to obtain optimal amounts of the aforementioned compounds. In this context, it may be important to evaluate the changes that occur during ripening using rapid analytical methods to decide the optimal harvest time.

Hyperspectral imaging is an emerging and rapid technique for nondestructive food analysis usually carried out in either the visible-short near-infrared (vis-NIR; 400–1000 nm) or near-infrared (NIR; 1000–1700 nm) spectral region.<sup>16</sup> The use of hyperspectral analysis has risen considerably in the food sector in the recent past.<sup>16–19</sup> Specifically, hyperspectral image analysis in the vis-NIR (400–1000 nm) and adaptive boosting neural networks have been used to determine anthocyanins in Cabernet Sauvignon

grape, obtaining promising results.<sup>20</sup> Nonetheless, classic NIR spectroscopy has been used in the enological sector to determine parameters in grapes such as gluconic acid, glycerol, soluble solids, and pH in grape juice,<sup>21</sup> total polyphenols, extractable anthocyanins, concentration of sugars, density,<sup>22</sup> total anthocyanins,<sup>23,24</sup> and the main families of phenolic compounds.<sup>25</sup> Therefore, it would be necessary to pay attention to the aforementioned electromagnetic range in the development of hyperspectral imaging methods in grapes because NIR spectroscopy has been proved to be a powerful analytical tool to determine bioactive compounds in a number of foodstuffs.<sup>26</sup>

The aim of this study was to evaluate the potential of near-infrared hyperspectral imaging for the screening of anthocyanins in grapes during ripening. To our knowledge, this is the first time that near-infrared hyperspectral imaging has been applied to grapes for this purpose.

## ■ MATERIAL AND METHODS

**Samples.** *Vitis vinifera* L. cv. Tempranillo and Syrah red grape samples were collected from two vineyards located in the Condado de Huelva Designation of Origin (D.O.) (Andalusia, Spain), which is under the typical climatic conditions of a warm area.<sup>8</sup> Red grapes were collected at different developmental stages during berry maturity in the 2012 vintage: prior to veraison (July 16) to over-ripening (September 6). Sixteen dates were taken into account for Tempranillo and 17 for Syrah. Three groups of berries per vineyard were collected at each date. Berries were collected from the top, middle, and bottom of the cluster and were immediately frozen and stored at –20 °C until analyses were performed. Two subsamples were randomly taken from each sample, one for the HPLC analysis and the other for the hyperspectral analysis.

**Anthocyanin Extraction and Chromatographic Analysis.** Grape skins were then separated manually from the whole grapes.

**Received:** May 16, 2013

**Revised:** September 18, 2013

**Accepted:** September 22, 2013

**Published:** September 23, 2013

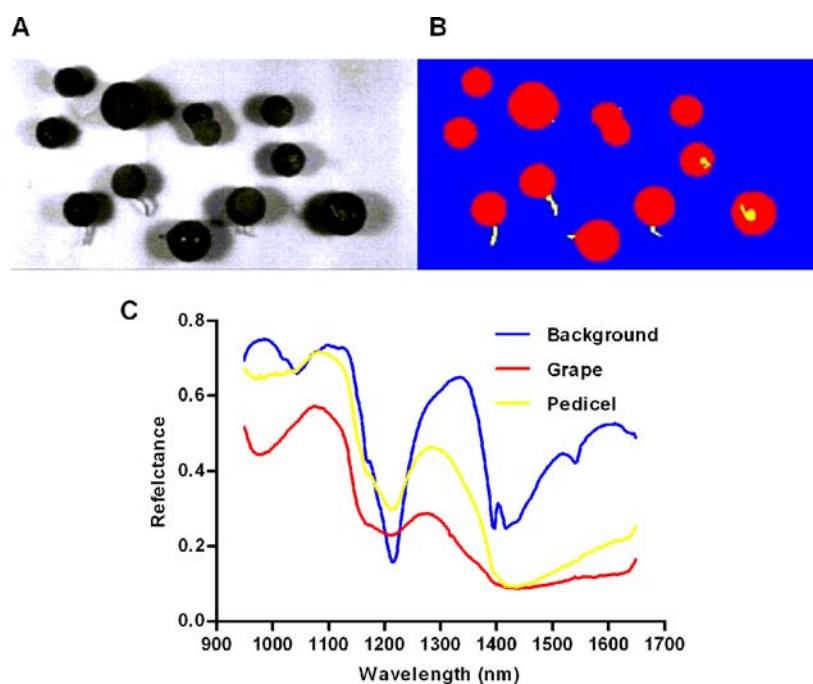


**Figure 1.** (A) Calibrated image at 1360 nm, (B) different parts of this image, and (C) the spectrum of each part.

One gram of grape skins was macerated at 4 °C in methanol containing 0.1% of 12 M HCl. Methanolic phases were centrifuged (3000 rpm, 10 min) and successively pooled, a few milliliters of water was added, and the extract was concentrated under vacuum at 30 °C until methanol was removed and finally made up to 10 mL with ultrapure water. The aqueous extract was diluted 1:2 with 0.1 M HCl, filtered through 0.45  $\mu\text{m}$  pore size filters, and directly injected into the chromatographic system to determine the anthocyanins.

Anthocyanin chromatographic analysis was carried out following a modification of the method of García-Marino et al.<sup>27</sup> Chromatographic analyses were performed on a Hewlett-Packard 1200 series HPLC equipped with an autoinjector, a quaternary HPLC pump, a column heater, a diode array detector (DAD), and a data treatment station. A Zorbax SB C18 column (4.6 mm  $\times$  250 mm, 4.6  $\mu\text{m}$  particle size) thermostated at 35 °C was used. Solvents were (A) 0.1% trifluoroacetic acid and (B) 100% HPLC grade acetonitrile. The elution profile was as follows: 10% B for 3.25 min, from 10 to 15% B for 12.37 min, 15% B for 5.21 min, from 15 to 18% B for 5.21 min, from 18 to 30% B for 20.84 min, and from 30 to 35% B for 5.20 min. The flow rate was 0.8 mL  $\text{min}^{-1}$ , and the injection volume was 100  $\mu\text{L}$ . The preferred detection wavelength was 520 nm. Up to 15 anthocyanins were identified according to their spectroscopic and chromatographic features, which had been previously acquired.<sup>27</sup> Results were expressed as malvidin-3-*O*-glucoside equivalents. All analyses were performed in duplicate. The standard error was generally around 10%, so the error and degree of accuracy of the reference method was considered appropriate to use these data as reference values.

Total anthocyanins were expressed as the sum of the individual anthocyanins. Moreover, anthocyanins were grouped by taking into account their basic structures. Total anthocyanin contents in the grape samples ranged from 0 to 23.8 mg  $\text{g}^{-1}$  grape skin with a standard deviation value of 5.6 mg  $\text{g}^{-1}$  grape skin. Nonacylated anthocyanin contents in the grape samples ranged from 0 to 16.9 mg  $\text{g}^{-1}$  grape skin with a standard deviation value of 3.9 mg  $\text{g}^{-1}$  grape skin. Acylated anthocyanins could be calculated as the difference between total and nonacylated anthocyanins.

**Hyperspectral Imaging Analysis.** The main components of the hyperspectral imaging device (Infaimon S.L., Barcelona, Spain) were the illumination source, optics (mirror scanner and lens), spectrograph, camera, and computer. The system comprised a Xenics XEVA-USB InGaAs camera (320  $\times$  256 pixels; Xenics Infrared Solutions,

Inc., Leuven, Belgium), a spectrograph (Specim ImSpector N17E Enhanced; Spectral Imaging Ltd., Oulu, Finland) covering the spectral range between 900 and 1700 nm (spectral resolution of 3.25 nm), two 70 W tungsten iodine halogen lamps (Prilux, Barcelona, Spain) mounted as source light, a mirror scanner (Spectral Imaging Ltd.), and a computer system. Hyperspectral images were recorded using a 50 Hz frame rate and an exposure time of 9 ms using the instrument acquisition software SpectralDAQ v. 3.62 (Spectral Imaging Ltd.). A two-point reflectance calibration was used. A Spectralon ceramic tile (Labsphere Inc., North Sutton, NH, USA) was used as a white reference, whereas dark current was recorded by taking a measurement after the spectrograph lens had been covered with a cup and the shutter closed.

Thereafter, the samples were thawed and tempered at room temperature, and the hyperspectral images of the intact grapes on a polyethylene plastic were recorded. The characteristic spectral profile of this surface was useful in the segmentation process for recognizing the region of interest. Only spectral data in the 950–1650 nm regions were used in data analysis due to reduced efficiency outside this range.

**Image Processing and Data Analysis.** *Image Processing.* Image treatment was carried out using Matlab (R2010b; The Math Works, Inc., Natick, MS, USA). Figure 1 shows a calibrated image at 1360 nm, different parts of this image, and the spectrum of each part. Prior to the quantitative analysis, a discriminant method was applied to the grape images to isolate the grapes from other parts of the image. First, three regions of interest (ROIs) were selected (background, grape, and pedicel) to develop a stepwise lineal discriminant model. The aforementioned discriminant model classified each pixel into two classes (grape or no grape pixel) using the reflectance values from six wavelengths (979, 1034, 1073, 1314, 1386, and 1550 nm). After that, the average spectrum of the grape region was extracted and then transformed into  $\log(1/R)$  units. The procedure was repeated for each sample, and the obtained spectra were combined into the spectral matrix. A flowchart of the image processing strategy employed in this study is shown in Figure 2.

*Data Analysis.* Prior to quantitative analysis, an unsupervised pattern recognition technique, principal component analysis (PCA), was used to provide information about the latent structure of the spectral matrix.<sup>28,29</sup>

Using the raw spectral data, testing different spectral pretreatments, and allocating the corresponding total anthocyanins or nonacylated

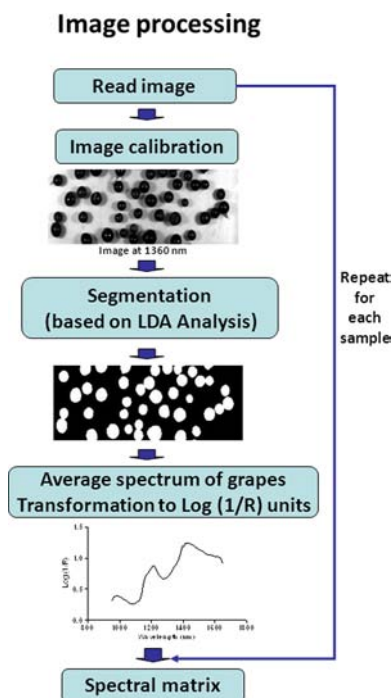


**Figure 2.** Flowchart of the data-processing strategy employed in this study.

anthocyanins values to each sample, calibrations were performed by modified partial least-squares regression (MPLS). In this method, the group of calibration samples is divided into a series of subsets to perform cross-validation to set the number of PLS factors, reduce the possibility of overfitting,<sup>28</sup> and remove chemical outliers. Using the  $T \geq 2.5$  criterion, samples that presented a high residual value when they were predicted were eliminated from the set. Finally, validation errors are combined into a single figure, the standard error of cross-validation (SECV).

Spectral pretreatments are usually applied to NIR raw data.<sup>30,31</sup> Moreover, the effect of derivatization and variations in spectral ranges were tested in the development of the NIRS calibrations.

The software used was Win ISI (v1.50) (Infrasoft International, LLC, Port. Matilda, PA, USA). From the three samples of each date, one (33%) was randomly allocated to the validation set and the other two (66%) to the calibration set. Consequently, from the 99 spectral samples, 66 were allocated in the calibration set and the remaining 33 were allocated in the validation set.

## RESULTS AND DISCUSSION

Figure 3 shows the average and standard deviation spectra of grapes over the 950–1650 nm range. Standard deviation spectra have been multiplied by a factor of 10 for display reasons. Spectral intensities were low and well within the linear response range of the instrument detector range. A strong feature of the sample spectra was the absorbance pattern around 1250 and 1450 nm wavelengths. The absorbance pattern around these wavelengths is mainly related to bands of the  $-\text{CH}$  and  $-\text{OH}$  functional groups, respectively.<sup>32</sup>

As part of the quantitative analysis, a standard normal variate (SNV 2,5,5,1) spectral pretreatment was applied to the aforementioned spectral range (i.e., 950–1650 nm) of samples in the calibration set. Mathematical treatment is denoted  $a,b,c,d$ , where the first digit is the number of the derivative, the second is the gap over which the derivative is calculated, the third is the number of data points in a running average or smoothing, and the fourth is the second smoothing.<sup>28</sup> After that, PCA was

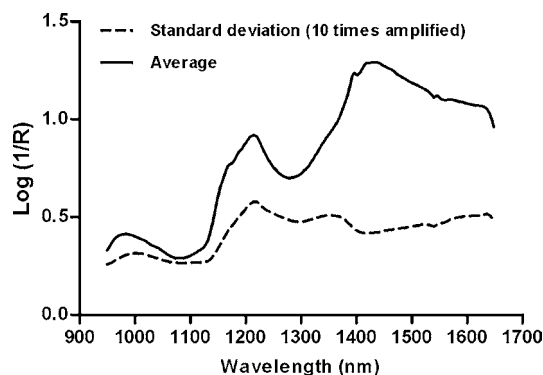


**Figure 3.** Average and standard deviation (10 times amplified) spectra of the whole group of grapes (99 samples) in the NIR zone between 950 and 1650 nm.

carried out to look for spectral outliers and create cross-validation groups. Overall, the spectral variability explained was 99% using 11 principal components, and Mahalanobis distances for each sample were calculated. Samples were ranked in order of their  $H$  (Mahalanobis) distance from the mean spectrum of the entire sample set, and the  $H > 3$  criterion was applied. No  $H$  outliers were found. Figure 4 shows the scores of the grape samples in the space defined by the first and second principal components, which described 49.47% (PC1) and 30.44% (PC2) of the variability in the data. In this plot, differences between the ripening stages are apparent (Figure 4A). Nevertheless, cultivars (i.e., Temepranillo and Syrah) were completely overlapped in this hyperspace (Figure 4B). The main difference observed in these plots was between ripening times, although the separation between stages was not complete. This trend in berry ripening was discernible on the basis of PC1.

Finally, quantitative calibrations were developed by MPLS regression using total or nonacylated anthocyanins as the dependent ( $Y$ ) variable and grape spectra as the independent ( $X$ ) variable. The statistical parameters of the final calibration equations are shown in Table 1, where  $N$  is the number of samples used to obtain the calibration equation after elimination of samples for chemical reasons ( $T$  criterion). The best of the different mathematical treatments, concentration range, and standard deviations are also shown. The average spectrum of the best of the different mathematically pretreated spectra is shown in Figure 5A. The robustness of the method has been checked by applying NIRS technology to 32 of 33 samples that did not belong to the calibration group. The remaining sample presented reference values outside the applicability of the obtained models and then should not be used in this procedure. Table 1 also shows the results obtained in the external validation, and the SEP values are presented. These values are comparatively similar to the errors previously reported for these compounds using classic NIR spectroscopy taking into account the applicability range.<sup>22–25</sup>

The biosynthesis of these compounds follows essentially the same course, so intercorrelations among them could be expected.<sup>33</sup> The correlations evidenced among these compounds show that it is not possible to ascertain if the results of NIRS models for predicting the composition nonacylated anthocyanins were due to their real absorbance or the correlation between nonacylated anthocyanins and total anthocyanins.

Figure 5B shows the loading plot of the MPLS model for total anthocyanin. The spectral regions around 1150 and 1400 nm show important contributions to the model loadings.

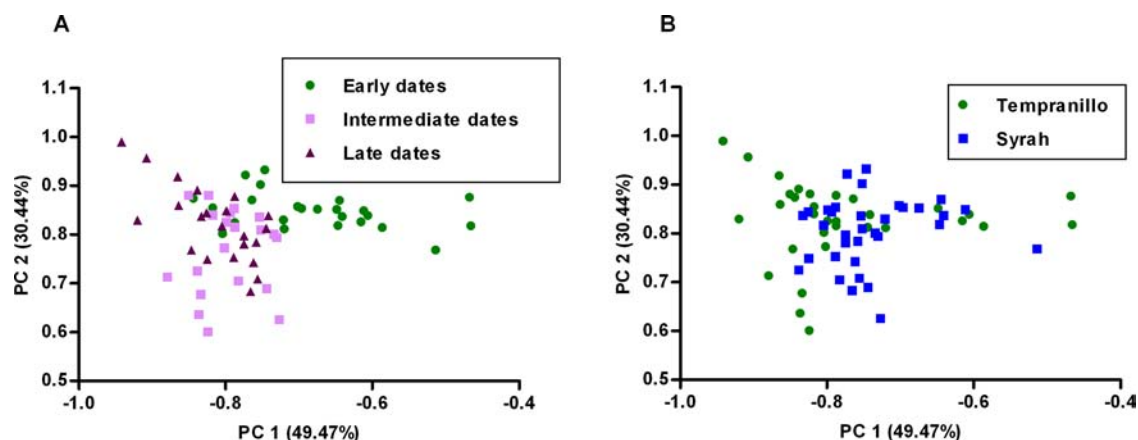


Figure 4. Score plots of grape samples (calibration set) in the space defined by PC1 and PC2.

Table 1. Calibration Statistical Descriptors for the Models Developed in the NIR Zone Close to 950–1650 nm

spectral pretreatment	compound	T outliers	PLS factors	$N^a$	mg g <sup>-1</sup> skin				RSQ <sup>d</sup>	mg g <sup>-1</sup> skin	
					est min	SD <sup>b</sup>	est max	SEC <sup>c</sup>		SECV <sup>e</sup>	SEP <sup>f</sup>
SNV 2,5,5,1	nonacylated anthocyanins	4	5	62	0	3.42	15.61	1.27	0.86	1.70	2.62
SNV 2,5,5,1	total anthocyanins	3	5	63	0	4.95	22.82	1.84	0.86	2.41	3.05

<sup>a</sup> $N$ , number of samples (calibration set). <sup>b</sup>SD, standard deviation. <sup>c</sup>SEC, standard error of calibration. <sup>d</sup>RSQ, coefficient of determination (calibration set). <sup>e</sup>SECV, standard error of cross-validation. <sup>f</sup>SEP, standard error of prediction (external validation).

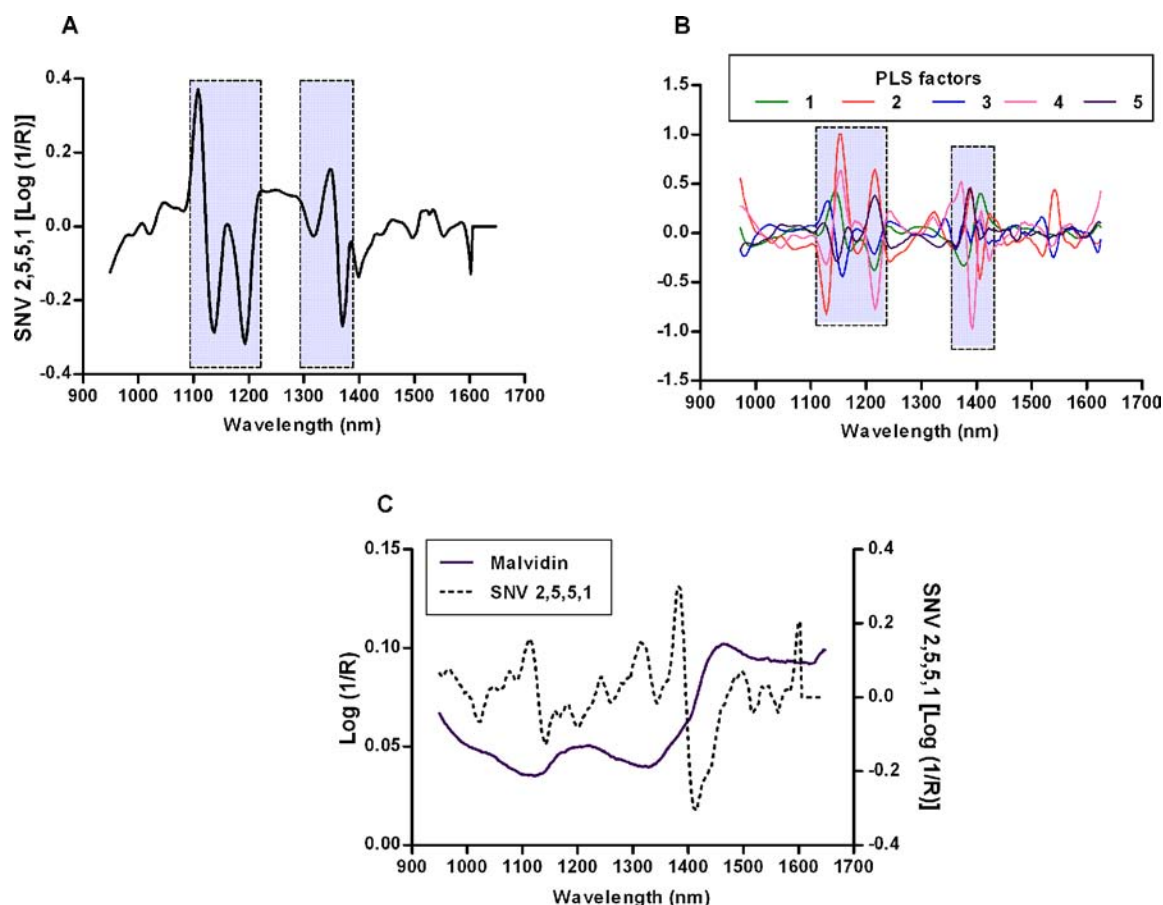


Figure 5. (A) Average spectrum of the best of the different pretreatments (SNV 2,5,5,1). (B) Loading plots of the MPLS model for total anthocyanins prediction. (C) Malvidin-3-*O*-glucoside and its second-derivative spectra.

These could be related to combination bands of the –OH functional group and symmetric and antisymmetric stretching.

This wavelength region is also related to C–H aromatic second overtones and C–H third overtones. These can be attributed

to the chemical structure of the compounds analyzed.<sup>32,34</sup> Malvidin-3-O-glucoside and its second-derivative spectra are shown in Figure 5C. Considerable spectral details are shown in the aforesaid wavelength range. This confirms previous studies that showed important contributions in the aforementioned spectral zones for determining anthocyanins.<sup>25</sup>

The potential of near-infrared hyperspectral imaging for the screening of total or nonacylated anthocyanins in intact red grapes was examined. A number of spectral pretreatments and different mask development strategies were studied to develop the quantitative models. The procedure reported here presents a good potential for a fast and reasonably inexpensive screening of these compounds. Nonetheless, a comprehensive study should be made to evaluate factors, such as different production areas and grape varieties, in the complete development of these models.

## AUTHOR INFORMATION

### Corresponding Author

\*(F.J.H.) Phone: +34 9545 56495. Fax: +34 9545 56110. E-mail: heredia@us.es.

### Funding

J.N.-B. and F.J.R.-P. thank the Spanish MICINN for FPI grants (BES-2012-060192 and BES-2009-025429, respectively). J.M.H.-H. is grateful for a Juan de la Cierva contract (JCI-2011-09201) and Project AGL2011-30254-C02. We also thank the Junta de Andalucía for financial support (Project P10-AGR6331).

### Notes

The authors declare no competing financial interest.

## REFERENCES

- (1) Crozier, A.; Clifford, M. N.; Ashihara, H. *Plant Secondary Metabolites. Occurrence, Structure and Role in the Human Diet*; Blackwell Publishing: Oxford, UK, 2006.
- (2) Koes, R. E.; Quattrocchio, F.; Mol, J. N. M. The flavonoid biosynthetic pathway in plants: function and evolution. *BioEssays* **1994**, *16*, 123–132.
- (3) Boulton, R. The copigmentation of anthocyanins and its role in the color of red wine: a critical review. *Am. J. Enol. Vitic.* **2001**, *52*, 67–87.
- (4) Moreno-Arribas, M. V.; Polo, C. *Wine Chemistry and Biochemistry*; Springer: New York, 2008.
- (5) Escribano-Bailón, M. T.; Santos-Buelga, C. Anthocyanin copigmentation – evaluation, mechanisms and implications for the colour of red wines. *Curr. Org. Chem.* **16**, 715–723.
- (6) Martín Bueno, J.; Ramos-Escudero, F.; Sáez-Plaza, P.; Muñoz, A. M.; Navas, M. J.; García Asuero, A. Analysis and antioxidant capacity of anthocyanin pigments. Part I: General considerations concerning polyphenols and flavonoids. *Crit. Rev. Anal. Chem.* **2012**, *42*, 102–125.
- (7) Coombe, B. G. The regulation of set and development of the grape berry. *Acta Hort.* **1973**, *34*, 261–273.
- (8) Gordillo, B.; Rodríguez-Pulido, F. J.; Mateus, N.; Escudero-Gilete, M. L.; González-Miret, M. L.; Heredia, F. J.; de Freitas, V. Application of LC-MS and tristimulus colorimetry to assess the ageing aptitude of Syrah wine in the Condado de Huelva D.O. (Spain), a typical warm climate region. *Anal. Chim. Acta* **2012**, *732*, 162–171.
- (9) Mira de Orduña, R. Climate change associated effects on grape and wine quality and production. *Food Res. Int.* **2010**, *43*, 1844–1855.
- (10) Ryan, J.-M.; Revilla, E. Anthocyanin composition of Cabernet Sauvignon and Tempranillo grapes at different stages of ripening. *J. Agric. Food Chem.* **2003**, *51*, 3372–3378.
- (11) Esteban, M. A.; Villanueva, M. J.; Lissarrague, J. R. Effect of irrigation on changes in the anthocyanin composition of the skin of cv Tempranillo (*Vitis vinifera* L.) grape berries during ripening. *J. Sci. Food Agric.* **2001**, *81*, 409–420.
- (12) Downey, M.; Dokoozlian, N. K.; Krstic, M. P. Cultural practice and environmental impacts on the flavonoid composition of grapes and wine: a review of recent research. *Am. J. Enol. Vitic.* **2006**, *57*, 257–268.
- (13) Guidoni, S.; Ferrandino, A.; Novello, V. Climate and agronomical practice effects on anthocyanin accumulation in cv. 'Nebbiolo' (*Vitis vinifera* L.) berries. *Am. J. Enol. Vitic.* **2008**, *59*, 22–29.
- (14) Ferrer-Gallego, R.; Hernández-Hierro, J. M.; Rivas-Gonzalo, J. C.; Escribano-Bailón, M. T. Influence of climatic conditions on the phenolic composition of *Vitis vinifera* L. cv. Graciano. *Anal. Chim. Acta* **2012**, *732*, 73–77.
- (15) Mori, K.; Sugaya, S.; Gemma, H. Decreased anthocyanin biosynthesis in grape berries grown under elevated night temperature condition. *Sci. Hortic.* **2005**, *105*, 319–330.
- (16) Gowen, A. A.; O'Donnell, C. P.; Cullen, P. J.; Downey, G.; Frias, J. M. Hyperspectral imaging – an emerging process analytical tool for food quality and safety control. *Trends Food Sci. Technol.* **2007**, *18*, 590–598.
- (17) Lorente, D.; Aleixos, N.; Gómez-Sanchis, J.; Cubero, S.; García-Navarrete, O.; Blasco, J. Recent advances and applications of hyperspectral imaging for fruit and vegetable quality assessment. *Food Bioprocess Technol.* **2012**, *5*, 1121–1142.
- (18) Sun, D. W. *Hyperspectral Imaging for Food Quality Analysis and Control*; Elsevier Science and Technology: San Diego, CA, USA, 2010.
- (19) Burger, J.; Gowen, A. A. Data handling in hyperspectral image analysis. *Chemom. Intell. Lab. Syst.* **2011**, *108*, 13–22.
- (20) Fernandes, A. M.; Oliveira, P.; Moura, J. P.; Oliveira, A. A.; Falco, V.; Correia, M. J.; Melo-Pinto, P. Determination of anthocyanin concentration in whole grape skins using hyperspectral imaging and adaptive boosting neural networks. *J. Food Eng.* **2011**, *105*, 216–226.
- (21) Versari, A.; Parpinello, G. P.; Mattioli, A. U.; Galassi, S. Determination of grape quality at harvest using Fourier-transform mid-infrared spectroscopy and multivariate analysis. *Am. J. Enol. Vitic.* **2008**, *59*, 317–322.
- (22) Kempes, B.; Leon, L.; Best, S.; De Baerdemaeker, J.; De Ketelaere, B. Assessment of the quality parameters in grapes using VIS/NIR spectroscopy. *Biosyst. Eng.* **2010**, *105*, 507–513.
- (23) Cozzolino, D. Near infrared spectroscopy in natural products analysis. *Planta Med.* **2009**, *75*, 746–756.
- (24) Cozzolino, D.; Damberg, R. G.; Janik, L.; Cynkar, W. U.; Gishen, M. Review: Analysis of grapes and wine by near infrared spectroscopy. *J. Near Infrared Spectrosc.* **2006**, *14*, 279–289.
- (25) Ferrer-Gallego, R.; Hernández-Hierro, J. M.; Rivas-Gonzalo, J. C.; Escribano-Bailón, M. T. Determination of phenolic compounds of grape skins during ripening by NIR spectroscopy. *LWT-Food Sci. Technol.* **2011**, *44*, 847–853.
- (26) McGoverin, C. M.; Weerananantaphan, J.; Downey, G.; Manley, M. Review: The application of near infrared spectroscopy to the measurement of bioactive compounds in food commodities. *J. Near Infrared Spectrosc.* **2010**, *18*, 87–111.
- (27) García-Marino, M.; Hernández-Hierro, J. M.; Rivas-Gonzalo, J. C.; Escribano-Bailón, M. T. Colour and pigment composition of red wines obtained from co-maceration of Tempranillo and Graciano varieties. *Anal. Chim. Acta* **2010**, *660*, 134–142.
- (28) Shenk, J. S.; Westerhaus, M. O. *Routine Operation, Calibration, Development and Network System Management Manual*; NIRSystems: Silver Spring, MD, USA, 1995; p 239.
- (29) Brereton, R. G. *Chemometrics: Data Analysis for the Laboratory and Chemical Plant*; Wiley: Chichester, UK, 2003; p 489.
- (30) Geladi, P.; MacDougall, D.; Martens, H. Linearization and scatter-correction for near-infrared reflectance spectra of meat. *Appl. Spectrosc.* **1985**, *39*, 491–500.
- (31) Dhanoa, M. S.; Lister, S. J.; Barnes, R. J. On the scales associated with near-infrared reflectance difference spectra. *Appl. Spectrosc.* **1995**, *49*, 765–772.
- (32) Osborne, B. G.; Fearn, T.; Hindle, P. T. *Practical NIR Spectroscopy with Applications in Food and Beverage Analysis*; Longman Scientific and Technical, Wiley: Harlow, UK, 1993; p 224.

(33) Harborne, J. B. *The Flavonoids: Advances in Research Since 1986*; Chapman and Hall: London, UK, 1993.

(34) Siesler, H. W.; Ozaky, Y.; Kawata, S.; Heise, H. M. *Near Infrared Spectroscopy: Principles, Instruments, Applications*; Wiley-VCH: Weinheim, Germany, 2002; p 348.